THE JOURNAL OF PHYSICAL CHEMISTRY B

 VOLUME 108, NUMBER 26, JULY 1, 2004

LETTERS

Linear and Nonlinear Optical Response of Silver Nanoprisms: Local Electric Fields of Dipole and Quadrupole Plasmon Resonances

Noriyuki Okada,[†] Yasushi Hamanaka,[†,‡] Arao Nakamura,*[,†,‡] Isabel Pastoriza-Santos,[§] and Luis M. Liz-Marzán*[,§]

Department of Applied Physics, Nagoya University, Chikusa-ku, Nagoya 464-8603, Japan, Core Research for Evolutional Science and Technology (CREST), Japan Science and Technology Agency, Shibuya-ku, Tokyo 150-0002, Japan, and Departamento de Química Física, Universidade de Vigo, 36200 Vigo, Spain

Received: April 26, 2004; In Final Form: May 20, 2004

By means of femtosecond pump and probe spectroscopy, linear and nonlinear optical properties of silver nanoprisms have been investigated, focusing on enhancement of local electric fields due to dipole and quadrupole surface plasmons. Ag nanoprsims were prepared by direct reduction of $AgNO_3$ by the solvent *N*,*N*-dimethylformamide in the presence of poly(vinylpyrrolidone). The average edge length and thickness of the nanoprisms (triangles and truncated triangles) were 67 and 35 nm, respectively. In the absorption spectra, dipole and quadrupole plasmon resonance bands have been observed. The values of the imaginary part of nonlinear susceptibility $\mathrm{Im}\chi^{(3)}$ measured at the dipole and quadrupole plasmon bands are -5.7×10^{-15} and -3.0×10^{-15} esu, respectively. The local electric field factors f_Q and f_D of quadrupole and dipole plasmon resonances were obtained from the observed dispersion curve of $\mathrm{Im}\chi^{(3)}$ and absorption spectra, yielding a ratio f_Q/f_D of ~0.7. The nonlinear response times of both resonances were found to be ~2 ps, which is close to the value for spherical nanoparticles, indicating that the relaxation process via electron−phonon interaction is governed by bulk crystal properties.

Introduction

Optical properties of metal nanoparticles have been of great interest for a long time, not only because of the beautiful colors of stained glass[1] but also because of other aspects as materials properties with applications for instance in photocatalysis[2] and in linear and nonlinear optical devices.[3−7] Recent technologies as diverse as e-beam lithography and wet chemistry have enabled the fabrication of nanoparticles with controlled shape and size, but particularly rods[8−13] and triangles,[14−17] as well as spherical nanoparticles[18−20] with well-defined sizes. Jin et al. have developed a photoinduced method for converting large quantities of silver nanospheres into nanoprisms, showing a change in color during progression of the conversion process.[14] Recently, we have reported a novel procedure for the synthesis of anisotropic Ag nanoparticles based on the use of *N*,*N*-dimethylformamide (DMF) as a solvent and as a reducing agent, in the presence of the polymer poly(vinylpyrrolidone) (PVP).[12,15]

In the case of spherical nanoparticles embedded in dielectric materials, the Mie scattering theory has succeeded to describe extinction spectra in the visible region, including the surface plasmon resonance of dipole modes, which result in strong attenuation of incident light.[21] The linear optical properties of nanospheres in a nonabsorbing medium can be quantitatively predicted by effective medium theories. In particular, the

* Corresponding authors.
[†] Nagoya University.
[‡] CREST, Japan Science and Technology Agency.
[§] Universidade de Vigo.

10.1021/jp048193q CCC: $27.50
Published on Web 06/02/2004

Maxwell−Garnett theory has been successfully applied to the calculation of nonlinear optical properties as well as the linear optical properties.[3,5,22,23] The surface plasmon resonance leads to large local electric fields, and such local fields result in enhancement of absorption coefficients and third-order nonlinear susceptibilities $\chi^{(3)}$ at the resonance frequency. The observed enhancement of $\chi^{(3)}$ as large as 10^{-7} esu around the surface plasmon resonance is well interpreted in terms of the local field effect.[5,6,24,25]

Recently, a considerable effort has been devoted to derive a theoretical interpretation of the linear optical response of nonspherical nanoparticles in which higher surface plasmon modes such as a quadrupole mode appear. Extinction spectra of perfect or truncated triangular Ag nanoprisms were numerically calculated using a discrete dipole approximation.[14,26] The extinction spectra show dipole and quadrupole plasmon resonances for both in-plane and out-of-plane polarizations. Surface plasmon resonances of Ag nanowires with a nonregular cross section have also been calculated by Kottmann et al.[27] Theoretical studies showed a dramatic localized enhancement of local electric fields at surface plasmon resonances in nonspherical nanoparticles. These local fields play a key role in nonlinear optical response, as well as surface enhanced Raman scattering. Experimentally, however, enhancement of $\chi^{(3)}$ due to the quadrupole plasmon resonance and a local field factor of this resonance have not yet been reported.

In this paper, we report on third-order nonlinear susceptibilities due to both the dipole and quadrupole plasmon resonances of Ag nanoprisms. We have measured linear and nonlinear absorption spectra using femtosecond pump−probe spectroscopy. Local field factors f_D and f_Q of dipole and quadrupole plasmon resonances were obtained from the observed absorption spectra and dispersion curve of $\chi^{(3)}$, yielding a ratio f_Q/f_D of 0.7. The characteristic times for the nonlinear optical response of both plasmon modes were also measured in the subpicosecond time region.

Experimental Section

Silver nanoprisms were prepared using a modification of a recently developed procedure[15] based on the use of *N*,*N*-dimethylformamide (DMF) as both a solvent and a reducing agent, in the presence of poly(vinylpyrrolidone) (PVP). Briefly, 15 μL of a 0.4 M aqueous solution of $AgClO_4$ (Aldrich) was added to 13 mL of DMF (Fluka) containing 0.2 g of PVP (MW 40 000, Fluka) at 175 °C, to form small Ag nanoparticles. Once these Ag nuclei were formed (8 min at 175 °C), 0.57 mL of an aqueous solution of $AgNO_3$ (Aldrich) 0.12 M was added in steps (30 μL every 3 min) and then the reaction was stopped by cooling and removing excess PVP by centrifugation. Finally, the particles were redispersed in ethanol.

Scanning electron microscopy (SEM) was carried out with a Hitachi S-4300 cold field emission SEM, and particle shape and size distributions were measured from several SEM images. Thickness and lateral size of triangles and particles with other polygonal shapes were also measured by using atomic force microscopy in contact mode (TMX2100 Explorer). Transient absorption spectra were measured by a femtosecond pump and probe method with a 150 fs pulse from an amplified Ti:sapphire laser system.[23] The pump pulse energy was set to 3.12 eV (ω_{pump}) corresponding to the in-plane quadrupole plasmon resonance. The probe pulse was a white-continuum generated by self-phase modulation of a part of the output pulse. Degenerate and nondegenerate components $Im\chi^{(3)}(-\omega_{probe}: -\omega_{pump}, \omega_{pump}, \omega_{probe})$ of the imaginary part of $\chi^{(3)}$ at the probe frequency of ω_{probe} ($\omega_{pump} = \omega_{probe}$ or $\omega_{pump} \neq \omega_{probe}$) were deduced from differential absorption spectra measured with pump peak powers of 3−13 GW/cm^2.

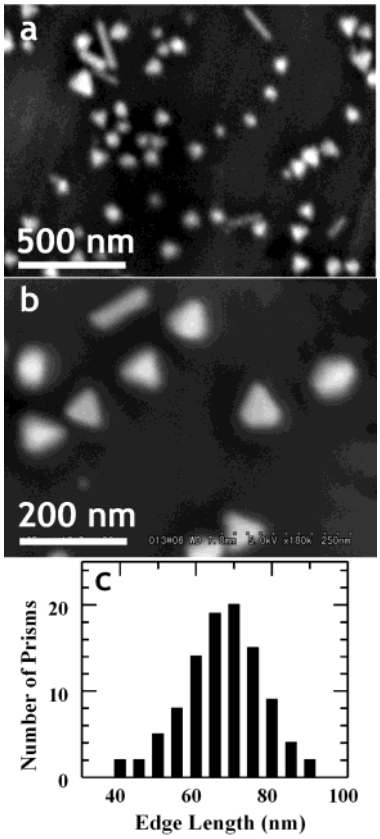

Figure 1. (a,b) SEM images of Ag nanoparticles in two different scales. (c) Histogram of edge length of Ag nanoprisms.

Results and Discussion

In Figure 1 (a and b) we show SEM images of the nanoparticles used in this study. The SEM image of Figure 1a shows nanoparticles with various shapes: triangles, rods, and polygonal shapes. However, statistically we have found that most of the nanoparticles are either perfect triangles or triangles truncated at each tip (Figure 1b). The presence of nanorods in the sample used for this study was found to be about 12% from the statistics of several SEM images. Figure 1c shows a histogram of the edge length of the triangles obtained from the measurement of about 100 particles. The edge length ranges between 40 and 90 nm, and assuming a Gaussian distribution the average and the standard deviation obtained are 67 and 11 nm, respectively. The average thickness measured by AFM is about 35 nm for the triangles. The average length and diameter of nanorods are 180 and 40 nm, respectively, and the aspect ratio is about 4.5.

Figure 2 shows the absorption spectrum of the same nanoprism sample characterized with SEM (see Figure 1). Three bands can be clearly identified within the photon energy region below the band-to-band transition energy (~4.3 eV). A calculation performed by Jin et al.[14] for perfectly triangular prisms and triangular prisms truncated at each tip has shown surface plasmon bands corresponding to dipole and quadrupole plasmon excitations. Comparing the observed spectrum to the calculation, we can attribute the lowest energy band (2.50 eV) to the in-plane dipole resonance, the band at 3.15 eV to the in-plane quadrupole resonance and the highest energy band (3.50 eV)

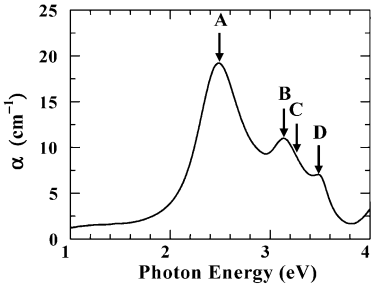

Figure 2. Absorption spectrum of Ag nanoprisms at room temperature. A: in-plane dipole resonance, B: in-plane quadrupole resonance, C: out-of-plane dipole resonance, D: out-of-plane quadrupole resonance.

to the out-of-plane quadrupole resonance. The out-of-plane dipole resonance is only observed as a shoulder in the calculation, and indeed this resonance is not observed as a clear band around 3.2 eV.

Although nanorods coexist with triangular prisms in the sample, the effect of the nanorods on the absorption spectrum is negligible. We calculated surface plasmon energies of nanorods with aspect ratios between 3 and 6 using the theory derived by Gans.[28] The resonance bands in the long axis and short axis directions appear at about 1.5 and 3.4 eV, respectively, for the nanorod with the aspect ratio of 4.5. The stronger resonance band in the long axis direction cannot be observed in the experimental absorption spectrum, and thus we can conclude that the contribution of nanorods to the absorption spectrum can be neglected.

Within the framework of the Maxwell−Garnett theory the electric field E_l, which the metal nanoparticles in the composite (the dispersion, in this case) see is related to the incident electric field E_o by

$$E_l = f_l E_o \tag{1}$$

where f_l is the local field factor.[3,5] We extend this relation to the case of the quadrupole plasmon resonance. Using an imaginary part ϵ_m'' of the dielectric function ϵ_m of the metal nanoparticles and a volume fraction of nanoparticles p, the absorption coefficient α_D (α_Q) at the dipole resonance frequency ω_D (quadrupole resonance frequency ω_Q) is given by

$$\alpha_i = p\frac{\omega_i}{nc}|f_i|^2\epsilon_m'' \tag{2}$$

where i = D or Q, c is the speed of light, f_D (f_Q) is the local field factor at the dipole resonance frequency (quadrupole resonance frequency), and n is the refractive index of the composite. In the case of Ag nanoparticles, the band-to-band transition energy (~4.3 eV) is well above the surface plasmon resonance energies. Consequently, ϵ_m'' is approximately constant in the vicinity of the surface plasmon resonance and n is also constant at the photon energy (or frequency) concerned. Therefore, the ratio α_Q/α_D is given by the following equation,

$$\frac{\alpha_Q}{\alpha_D} = \frac{\omega_Q}{\omega_D}\frac{|f_Q|^2}{|f_D|^2} \tag{3}$$

From this relation we can estimate a ratio f_Q/f_D between the local field factor at the quadrupole resonance frequency and that at the dipole resonance frequency. Taking the measured ratio α_Q/α_D as 0.57, we obtained an f_Q/f_D ratio of 0.67.

Nonlinear absorption spectra and values of $\mathrm{Im}\chi^{(3)}$ were measured using the pump and probe technique. Figure 3 shows

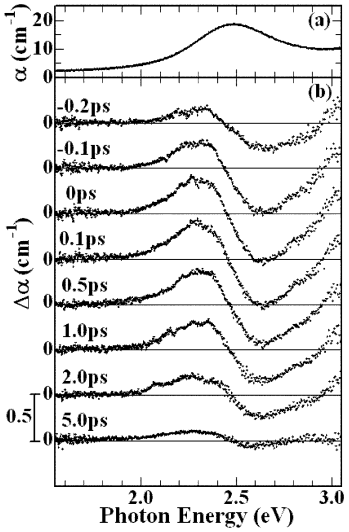

Figure 3. Absorption spectrum (a) and differential absorption spectra (b) for different delay times between pump and probe pulses shone through a dispersion of Ag nanoprisms at room temperature.

the linear absorption spectrum and the differential absorption spectra ($\Delta\alpha$) measured in the spectral range between 1.55 and 3.05 eV with a pump photon energy of 3.12 eV. The pump photon energy corresponds to the in-plane quadrupole resonance. $\Delta\alpha$ shows a decrease at the high-energy side of the in-plane dipole resonance band and an increase at the low-energy side. The observed features of the differential spectra suggest a red-shift of the dipole resonance band. An increase in absorption observed above 2.95 eV is related to the in-plane quadrupole resonance, though the signal above 3.05 eV corresponding to the resonance band cannot be detected because of the leakage of the pump pulse light. Shown in Figure 3b are the differential absorption spectra with various delay times between pump and probe pulses. As the delay time is increased, $\Delta\alpha$ decreases, but the spectral features remain constant.

Using the Maxwell−Garnett theory for the dielectric function of the composite system, the nondegenerate component of $\chi^{(3)}$ of metal nanoparticle composites can be represented by the third-order susceptibility $\chi_m^{(3)}$ of the bulk metal:[3,5]

$$\chi^{(3)}(\omega_{probe}) = pf_l^2(\omega_{probe})|f_l(\omega_{pump})|^2\chi_m^{(3)}(\omega_{probe}) \tag{4}$$

Under our experimental conditions of ω_{pump} = 3.12 eV, $|f_l(\omega_{pump})|$ is equal to the local field factor $|f_Q|$ at the in-plane quadrupole resonance frequency ω_Q. For moderate laser intensities, I, the change in the absorption coefficient is described by $\Delta\alpha = \beta I$, where β is a nonlinear absorption coefficient. β is related to $\mathrm{Im}\chi^{(3)}$ by

$$\mathrm{Im}\chi^{(3)}(-\omega_{probe}: -\omega_{pump}, \omega_{pump}, \omega_{probe}) = \frac{n^2c^2}{240\pi^2\omega_{probe}}\beta \tag{5}$$

Therefore, we can estimate $\mathrm{Im}\chi^{(3)}$ values from the dependence of $\Delta\alpha$ on I.[29] In Figure 4a, $\Delta\alpha$ values measured at 2.30 eV and 0.1 ps are plotted as a function of the intensity of the pump pulse I. $\Delta\alpha$ increases linearly with I. From the linear least-squares fit, a value for β is obtained of $(6.1 \pm 0.8) \times 10^{-13}$ m/W which yields $\mathrm{Im}\chi^{(3)}$ of $(1.2 \pm 0.2) \times 10^{-14}$ esu. Here, we used $n = 1.36$ which is the refractive index of ethanol, because the concentration of nanoparticles in ethanol is low. For the negative peak at 2.65 eV in the differential absorption spectra,

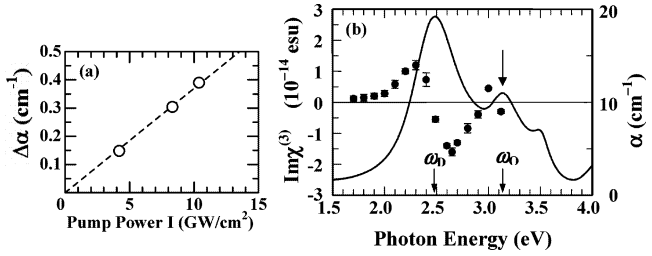

Figure 4. (a) Change in absorpion coefficient $\Delta\alpha$ measured at 2.30 eV and 0.1 ps as a function of the pump pulse intensity. The dotted line is a linear fit to the data. (b) Absorption spectrum and dispersion curve of $\mathrm{Im}\chi^{(3)}$ in Ag nanoprisms at room temperature. The arrow indicates the photon energy of the pump pulse for the measurements of $\mathrm{Im}\chi^{(3)}$. Arrows labeled with ω_D and ω_Q point to the dipole and quadrupole resonance peak frequencies, respectively.

$\mathrm{Im}\chi^{(3)}$ is $-(1.6 \pm 0.2) \times 10^{-14}$ esu, which is the maximum value in the vicinity of the dipole resonance frequency. For the in-plane quadrupole resonance we measured $\Delta\alpha$ using a probe pulse with the same photon energy (3.12 eV) as that of the pump pulse. The $\mathrm{Im}\chi^{(3)}$ value obtained at ω_Q is $-(3.0 \pm 0.6) \times 10^{-15}$ esu.

The $\mathrm{Im}\chi^{(3)}$ values obtained are summarized together with the absorption spectrum in Figure 4b. The $\mathrm{Im}\chi^{(3)}$ value is positive at the low-energy side and negative at the high-energy side of the dipole resonance band (2.50 eV). At the dipole resonance peak frequency, ω_D (2.50 eV), $\mathrm{Im}\chi^{(3)}$ is negative, with a value of -5.7×10^{-15} esu. A similar feature is observed for the quadrupole resonance: the $\mathrm{Im}\chi^{(3)}$ value is positive at the low-energy side and negative at the high energy side of the band. The $\mathrm{Im}\chi^{(3)}$ values at the dipole ($\mathrm{Im}\chi_D^{(3)}$) and quadrupole ($\mathrm{Im}\chi_Q^{(3)}$) resonance peak frequencies are thus -5.7×10^{-15} esu and -3.0×10^{-15} esu, respectively. The ratio $\mathrm{Im}\chi_Q^{(3)}/\mathrm{Im}\chi_D^{(3)}$ is also related to the local field factors f_Q and f_D. Under our experimental conditions, $\chi_Q^{(3)}$ at ω_Q and $\chi_D^{(3)}$ at ω_D can be expressed through the following expressions:

$$\chi_Q^{(3)} = p f_Q{}^2 |f_Q|^2 \chi_m^{(3)}$$
$$\chi_D^{(3)} = p f_D{}^2 |f_Q|^2 \chi_m^{(3)} \qquad (6)$$

Taking into account that the real part of $\chi^{(3)}$ is extremely small compared to $\mathrm{Im}\chi^{(3)}$ at resonance,[23] the ratio $\mathrm{Im}\chi_Q^{(3)}/\mathrm{Im}\chi_D^{(3)}$ is given by

$$\mathrm{Im}\chi_Q^{(3)}/\mathrm{Im}\,\chi_D^{(3)} \approx f_Q{}^2/f_D{}^2 \qquad (7)$$

Using the measured value of the ratio $\mathrm{Im}\chi_Q^{(3)}/\mathrm{Im}\chi_D^{(3)}$ (0.53), the ratio f_Q/f_D obtained is 0.73. This value is in good agreement with the value obtained from the ratio of the absorption coefficients within the experimental error. Therefore, the local field factor of the quadrupole plasmon resonance is 0.7 times that of the dipole plasmon resonance for Ag nanoprisms consisting of a mixture of perfect triangles and triangles truncated at each tip. In this enhancement of the local field, the contribution of band-to-band transition is not included, because the transition energy ($\sim$4.3 eV) is situated far away from the surface plasmon resonances. To investigate surface plasmon related phenomena,[23,29] this is actually an advantage of Ag over Au and Cu nanoparticles, in which the band-to-band transition ($\sim$2 eV) appears close to the surface plasmon resonance.

We now discuss the response time of optical nonlinearities due to the dipole and quadrupole resonances in Ag triangular prisms. The time evolutions measured at 2.65 and 3.12 eV with a pump fluence of about 2 mJ/cm^2 are shown in Figure 5. $\Delta\alpha$ exhibits exponential decay behavior; an exponential fit to the data yields for 2.65 and 3.12 eV relaxation times of 2.1 ± 0.4 and 1.7 ± 0.2 ps, respectively. The observed relaxation times for both cases are the same within the experimental error and are comparable to the values for spherical particles measured with a similar pump fluence.[30] The relaxation time of spherical particle−insulator composites can be successfully analyzed by means of the two-temperature model, which indicates the strong dependence of the relaxation time on the pump fluence. With a lower pump fluence the relaxation time becomes less than 1 ps because the initial temperature of the electron system heated by the pump pulse excitation is relatively low.[6,31] Using the two-temperature model,[6,30] an estimation of electron and lattice temperatures in triangular prisms for the pump fluence of 2 mJ/cm^2 yields about 1000 and 310 K, respectively. Consequently, the agreement between the relaxation times measured for triangular prisms and those for spherical particles is reasonably understood, taking into account that the relaxation time is determined by the cooling dynamics of hot electrons into the lattice system via the electron−phonon interaction in the particles. The electron−phonon coupling constant is a bulk crystal property and is independent of the nanoparticle shapes and the local electric field.

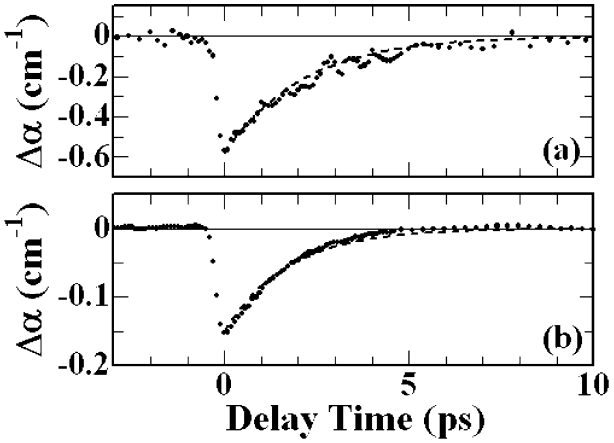

Figure 5. Time evolutions of the differential absorption $\Delta\alpha$ measured at 2.65 eV (a) and 3.12 eV (b). The dashed lines are exponential fits to the data.

Conclusions

We have investigated linear and nonlinear optical properties of Ag nanoprisms by means of femtosecond pump and probe spectroscopy. For Ag nanoprisms prepared by direct reduction of $AgNO_3$ by solvent DMF in the presence of PVP, over 85% of the nanoparticles were either triangles or truncated triangles with lateral sizes between 40 and 90 nm. In the absorption spectra, dipole and quadrupole plasmon resonance bands were observed, and from the ratio of absorption coefficients at both bands, a value of 0.67 was obtained for the ratio of the local field factor f_Q/f_D. The values of $\mathrm{Im}\chi^{(3)}$ at the dipole and quadrupole plasmon resonance frequencies are -5.7×10^{-15} and -3.0×10^{-15} esu, respectively, which yields a f_Q/f_D ratio of 0.73. Therefore, we have found that the local field enhancement of the quadrupole plasmon resonance is 0.7 times that of the dipole resonance. The nonlinear response times of both resonances were $\sim$2 ps, which is close to the value for spherical nanoparticles, indicating that the relaxation process via electron−phonon interaction is governed by bulk crystal properties.

Acknowledgment. The authors are grateful to I. Yamakawa for his assistance in SEM experiments. L.M.L.M. acknowledges financial support from the Spanish Ministerio de Ciencia y Tecnología (Project no. BQU2001-3799) and Xunta de Galicia (Project no. PGIDIT03TMT30101PR).

References and Notes

(1) Faraday, M. *Philos. Trans. Royal Soc. London* **1857**, *147*, 145.
(2) Kamat, P. V. *J. Phys. Chem. B* **2002**, *106*, 7729.
(3) Hache, F.; Ricard, D.; Flytzanis, C. *J. Opt. Soc. Am. B* **1986**, *3*, 1647.
(4) Haglund, R. F., Jr.; Yang, L.; Magruder, R. H., III; Wittig, J. E.; Becker, K.; Zuhr, R. A. *Opt. Lett.* **1993**, *18*, 373.
(5) Uchida, K.; Kaneko, S.; Omi, S.; Hata, C.; Tanji, H.; Asahara, Y.; Ikushima, A. J.; Tokizaki, T.; Nakamura, A. *J. Opt. Soc. Am. B* **1994**, *11*, 1236.
(6) Tokizaki, T.; Nakamura, A.; Kaneko, S.; Uchida, K.; Omi, S.; Tanji, H.; Asahara, Y. *Appl. Phys. Lett.* **1994**, *65*, 941.
(7) West, R.; Wang, Y.; Goodson, T., III *J. Phys. Chem. B* **2003**, *107*, 3419.
(8) Cepak, V. M.; Martin, C. R. *J. Phys. Chem. B* **1998**, *102*, 9985.
(9) Schoenenberger, C.; van der Zande, B. M. I.; Fokkink, L. G. J.; Henny, M.; Schmid, C.; Krueger, M.; Bachtold, A.; Huber, R.; Birk, H.; Staufer, U. *J. Phys. Chem. B* **1997**, *101*, 5497.
(10) Chang, S.-S.; Shih, C.-W.; Chen, C.-D.; Lai, W.-C.; Wang, C. R. C. *Langmuir* **1999**, *15*, 701.
(11) Jana, N. R.; Gearheart, L.; Murphy, C. J. *J. Phys. Chem. B* **2001**, *105*, 4065.
(12) Giersig, M.; Pastoriza-Santos, I.; Liz-Marzán, L. M. *J. Mater. Chem.* **2004**, *16*, 607.
(13) Nikoobakht, B.; El-Sayed, M. A. *Chem. Mater.* **2003**, *15* 1957.
(14) Jin, R.; Cao, Y.; Mirkin, C. A.; Kelly, K. L.; Schatz, G. C.; Zheng, J. G. *Science* **2001**, *294*, 1901.
(15) Pastoriza-Santos, I.; Liz-Marzán, L. M. *Nano Lett.* **2002**, *2*, 903.
(16) Chen, S.; Carroll, D. L. *Nano Lett.* **2002**, *2*, 1003.
(17) Malikova, N.; Pastoriza-Santos, I.; Schierhorn, M.; Kotov, N. A.; Liz-Marzán, L. M. *Langmuir* **2002**, *18*, 3694.
(18) Turkevich, J.; Stevenson, P. C.; Hillier, J. *Discuss. Faraday Soc.* **1951**, *11*, 55.
(19) Jana, N. R.; Gearheart, L.; Murphy, C. J. *Langmuir* **2001**, *17*, 6782.
(20) Brust, M.; Walker, M.; Bethell, D.; Schiffrin, D. J.; Whyman, R. *Chem. Commun.* **1994**, 801.
(21) Mie, G. *Ann. Phys.* **1908**, *25*, 377.
(22) Maxwell−Garnett, J. C. *Philos. Trans. R. Soc. London Ser A* **1904**, *203*, 385.
(23) Hamanaka, Y.; Nakamura, A.; Omi, S.; Del Fatti, N.; Vallee, F.; Flytzanis, C. *Appl. Phys. Lett.* **1999**, *75*, 1712.
(24) Halté, V.; Bigot, J.-Y.; Palpant, B.; Broyer, M.; Prével, B.; Pérez, A. *Appl. Phys. Lett.* **1999**, *75*, 3799.
(25) Olivares, J.; Requejo-Isidro, J.; del Coso, R.; de Nalda, R.; Solis, J.; Afonso, C. N.; Stepanov, A. L.; Hole, D.; Townsend, P. D.; Naudon, A. *J. Appl. Phys.* **2001**, *90*, 1064.
(26) Kelly, K. L.; Coronado, E.; Zhao, L. L.; Schatz, G. C. *J. Phys. Chem. B* **2003**, *107*, 668.
(27) Kottmann, J. P.; Martin, O. J. F.; Smith, D. R.; Schultz, S. *Phys. Rev. B* **2001**, *64*, 235402/1.
(28) Gans, R. *Ann. Phys.* **1915**, *47*, 271.
(29) Hamanaka, Y.; Nakamura, A.; Hayashi, N.; Omi, S. *J. Opt. Soc. Am. B* **2003**, *20*, 1227.
(30) Hamanaka, Y.; Kuwabata, J.; Tanahashi, I.; Omi, S.; Nakamura, A. *Phys. Rev. B* **2001**, *63*, *104302*.
(31) Arbouet, A.; Voisin, C.; Christofilos, D.; Langot, P.; Del Fatti, N.; Vallee, F.; Lerme, L.; Celep, G.; Cottancin, E.; Gaudry, M.; Pellarin, M.; Broyer, M.; Maillard, M.; Pileni, M. P.; Treguer, M. *Phys. Rev. Lett.* **2003**, *90*, 177401.